Pretest Analysis of a 1/4 Scale Prestressed Concrete Containment Vessel Model

Shiro Mitsugi[1)], Takako Kashiwase[2)], and Hideo Nagasaka[1)]

1) Nuclear Power Engineering Corporation, Tokyo, JAPAN
2) Obayashi Corporation, Tokyo, JAPAN

ABSTRACT

Nuclear Power Engineering Corporation (NUPEC), with US Nuclear Regulatory Commission (NRC), is conducting a program where an ultimate strength test of prestressed concrete containment vessel (PCCV) has been made on a 1/4 uniform scale model of an actual PCCV of a plant in Japan. The model had an equipment hatch, several penetrations, and liner with T-anchors. Prior to the test, a number of regulatory and research organizations were invited to participate in a pretest Round Robin to perform predictive analyses of the response of the model. The purpose of the pretest analyses is to establish analysis methods for PCCV by comparing its results with actual test results. This paper describes the analyses NUPEC performed as a participant of the Round Robin.

The pretest analyses, using ABAQUS Standard, deal with axisymmetric global model and some local models, such as wall-base junction model, equipment hatch model, and main steam nozzle model. The results of the axisymmetric global analysis serves as boundary conditions on the other local analyses, showing that stiffness-changing parts are likely to be ruptured. The results show the possibility of hoop tendon rupture at mid-height cylinder part or liner tearing around concrete thickness discontinuity.

1. GLOBAL ANALYSIS

1.1 Material Properties

The measured average data of concrete Young's modulus, Poisson's ratio, compressive strength, and tensile strength were used based on trial mix concrete tests after field curing. As for rebar, the average stress-strain curves of each size/type of rebar material tests were used. Some of the rebar test pieces were shaved in dumbbell shape, whose results were not included in the average. The average stress-strain curves obtained from liner material tests were also used, where isotropy of the liner was assumed. Mises yield condition was employed for the liner. The measured stress-strain curve of a tendon material test was used. Actual material properties used for the analyses are shown in the Round Robin report [1], [2].

1.2 Concrete Models

ABAQUS/Standard Ver. 5.8, a finite element program, was used for the analyses.

The stress-strain curve of post-cracking concrete was determined through a sensitivity study using the 1/6 RCCV test results conducted at SNL [3]. The tension stiffening linearly decreased aiming zero at the strain 10 times as large as the concrete crack strain, 1.28×10^{-4}. 1% of crack stress was, for calculation stability, retained after reaching ten times the crack strain.

The reduction of the shear modulus after concrete cracking was determined though another sensitivity study, and the results were compared between the model with full shear retention and the one with shear modulus reduction. The analysis results had been almost same, so that the full shear retention model was employed because of the better convergence in calculation.

Non-linear behavior in multi-axial stress field was set to be traced by crack detection surface and compressive surface incorporated in ABAQUS code. Except for the measured ratio of the tensile strength to the compressive strength, default values of parameters in ABAQUS were used where no biaxial test data were available.

1.3 Analytical Modeling

An axisymmetric global analysis was carried out as the first step of the pre-test analyses. The analytical model consisted of dome, cylinder, and basemat part. The wall-basemat juncture part was generated with finer elements than the surrounding portion. The model consisted of 1,963 nodes and 1,279 elements.

4 -node bilinear element (CAX4) was used for concrete. Rebar was modeled with REBAR element in solid element. Liner was modeled with shell element (SAX1). Liner nodes were shared in common with inside nodes of concrete.

The hoop tendon was modeled with rebar bonded to the concrete. Meridional tendon was modeled with shell element. Its stiffness in hoop direction was zero in the cylinder part, while it has hoop-direction stiffness in the dome part above 45 degrees because of its mesh-like layout in the part.

The meridional tendon was allowed to slide in the concrete. Friction coefficient at dome part was 0.2156, which

was the sum of μ=0.21 rad^{-1}, average value of the measured friction coefficient, and λ=0.001 m^{-1}, friction coefficient per length. For cylinder part, where the tendon were laid straight, μ=0 and λ=0.001 were used.

Non-linear soil springs were placed at the bottom of basemat to simulate subgrade reaction force. The actual ground stiffness of 30 MPa was used against compression force, and zero against tension force in uplift part. The soil springs in non-uplift part were set to have stiffness against tension force, because the vertical displacement became too large when all tensile stiffness of soil springs in non-uplift part were zero.

Gravity was concentrated to the bottom of basemat as concentrated force. Gravitational force at each node was neglected, because they were much smaller than tendon tensile force.

In order to simulate a setting loss condition of tendon, meridional tendon was prestressed with the design value of 503 kN and then loosed to the design value of 470 kN. As for hoop tendon, initial stress of 991 MPa, corresponding to the average value of hoop tendon stress, was loaded.

1.4 Analysis Results

Figure 1 shows global deformation behavior of the model. A slight inward deformation due to prestressing was observed when tendons were anchored after prestressing. The cylinder shape under 1.5 Pd became almost same as that before prestressing. (Pd: design pressure, 0.39 MPa) The dome part deformed inward slightly under the pressure. The mid-cylinder part began to deform outward from the original shape at 2.2 Pd, while the dome part still shrank. Outward deformation of the mid-cylinder part became remarkable at 3.6 Pd, when the dome part deformed downwards.

Figure 2 plots radial displacements. The point No. 4, the upper part of the mid-cylinder, showed the largest radial displacement, both the basemat and dome part constraining radial displacement of cylinder part. The displacements in the cylinder part, No. 3 and No. 4, increased linearly up to about 2.1 Pd, when hoop crack of the concrete (crack due to hoop stress) began as described below. The displacement increased drastically at about 3.5 Pd due to meridional crack of the concrete.

Figure 3 shows concrete cracking behavior in hoop and meridional directions. Hoop cracking initially occurred at 2.1 Pd. The hoop cracking caused the non-linear radial displacement shown in Fig. 2. The hoop cracking extended above spring line at 2.4 Pd, when the cylinder part deformed outward slightly as shown in Fig. 1. Although meridional cracking on outer surface extended to the whole cylinder part at 3.4 Pd, there was little inner surface cracking. Both hoop and meridional cracking almost extended to the whole region at

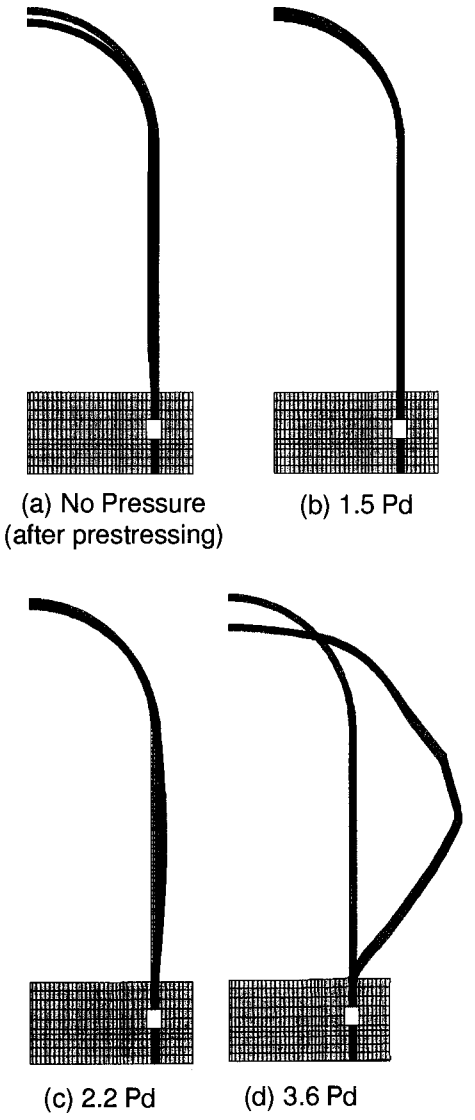

Fig. 1 Deformation of the Model

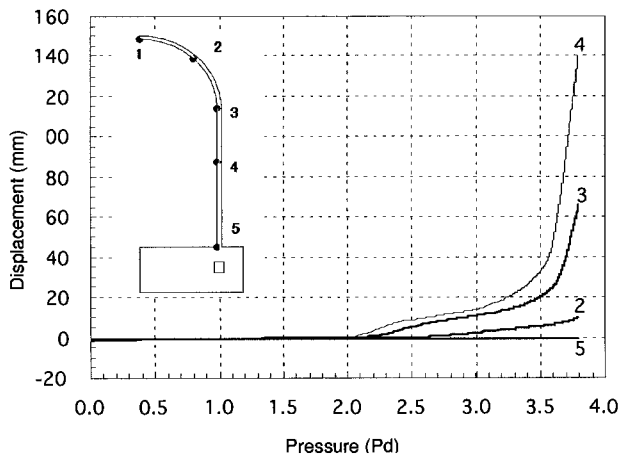

Fig. 2 Radial Displacements

3.6 Pd, when radial displacement increased drastically as shown in Fig. 2. Bending behavior was observed in the meridional direction; meridional cracking mainly occurred outside of concrete wall in the mid-height cylinder part.

Figure 4 is a plot of liner strain in hoop direction. Hoop liner strain remained negative up to about 1.5 Pd due to the prestress. Hoop rebar stresses exhibited similar behavior as shown in Fig. 5. The liner strain of mid-cylinder part (No. 4) increased non-linearly after about 2.1 Pd and increased drastically at around 3.5 Pd. They were closely related to the concrete cracking condition due to hoop stress at 2.1 and one due to meridional stress at 3.6 Pd as shown in Fig. 3. Similar strain behavior occurred at spring line (No. 3) and a dome part (No. 2); the strain level was lower than that in mid-cylinder part. The strain near basemat (No. 5) was almost zero because of the strong constraint force by the basemat. Hoop crack had extended to the whole region of the cylinder part at 3.4 Pd, and the rebar in cylinder part almost yielded at this pressure, as shown in Fig. 5 (yield stress: 459 MPa). That is, the change in liner strain was explained by the changes in concrete and rebar stiffness.

In summary, concrete cracking governed the global behavior of the model, that is, the reduction of concrete stress due to cracking caused the changes in stress distribution of rebars and tendons and resultant global deformation behavior.

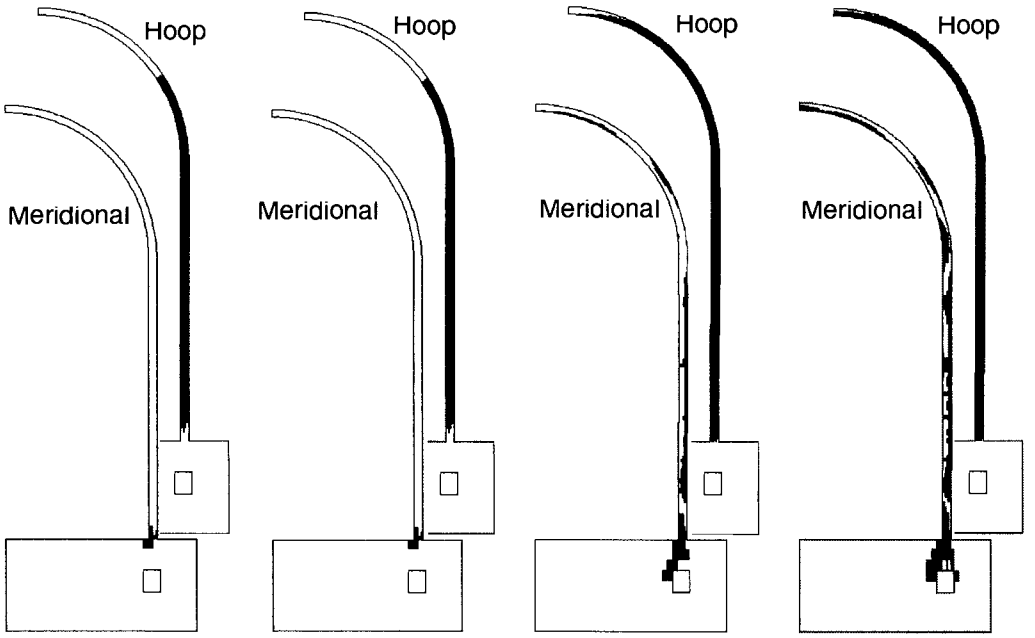

Fig. 3 Concrete Cracking

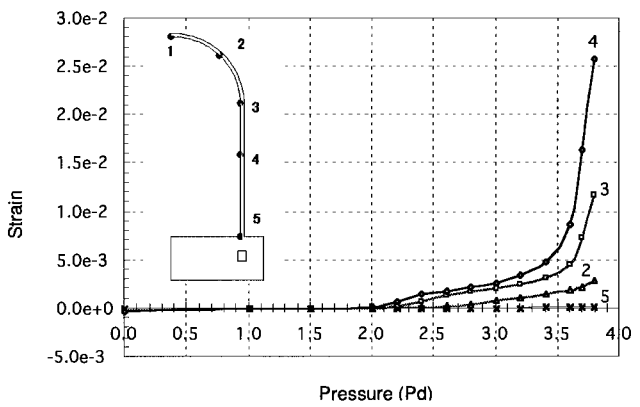

Fig. 4 Hoop Liner Strains

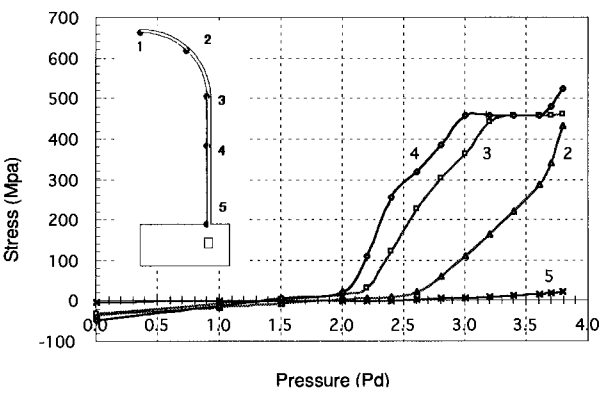

Fig. 5 Hoop Rebar Stresses

2. LOCAL ANALYSES

2.1 Selection of Failure Parts

Possible failure parts of 1/4 PCCV test model were investigated at its design stage. According to the investigation, potential failure parts were crane brackets, hatches, wall-base junction, buttress, spring line, and tendon gallery. 1/6 RCCV test demonstrated that liner tearing concentrated on the mid-cylinder part [3]. NUPEC's SCV shell model was failed by liner tearing at the junction of thick plate around a hatch [4]. Based on these two tests, there was a possibility of the 1/4 PCCV test model failing by liner tearing around hatches in the mid-cylinder part.

The global analysis results predicted that liner strain in the mid-cylinder part would be larger than those in other parts similar to the above studies and that outer concrete compressive stress at the wall-basemat juncture would also be large. Considering the all above results, several hatches in the mid-cylinder part and the junction between wall and basemat were considered as potential failure parts, and their analyses were conducted. Due to the limitation of space, the wall-basemat juncture model and two other models are focused in the present paper.

2.2 Failure Criteria

Compressive strength of concrete was set to be 42 MPa for Fc=300 concrete, which were used for the lower part of the basemat under the tendon gallery, and 49 MPa for Fc=450 concrete, which were used for the remaining portion of the basemat and all the other parts including dome and cylinder. They were based on the measured average data of concrete trial mix tests after 13 weeks field curing. It is well known that the concrete compressive strength normal to the initial concrete cracking direction is reduced [5]. The average of the reduction factor calculated by compressive field theory with the global analysis results was about 30%. Concrete body, however, is not totally failed by a local failure, so that the failure judgement should be decided considering the extent of failure region.

Nominal values from JIS (Japanese Industrial Standards) were used for rebar failure strain: 18% for SD345, 16% for SD390 and 12% for SD490.

While MITI (Ministry of International Trade and Industry) Notification No. 452 specifies nominal value of 2.0% strain for tendon failure criterion, the measured average data of failure strain was 3.8% in the tendon system tests performed. The tendon failure criterion was chosen as 3.0% due to the consideration on construction conditions at the site in field.

The average measured data of liner tearing strain was 33.5% and 33.0% in the hoop and meridional respectively according to the liner tensile test performed. Biaxial failure strain in containment vessel tests performed by NUPEC, were smaller than measured failure strain in uniaxial tensile tests [2], [4]. Failure criteria of liner was determined as 8% based on tearing strain of 1/6 RCCV which was similar to the 1/4 PCCV material and structure [3].

Table 1 shows summary of failure criteria.

Same material properties with the global analysis were used for all local analyses.

Table 1 Failure criteria

Material		Failure criteria	Base
Concrete	Fc=300 Fc=450	Compressive stress 42 MPa* Compressive stress 49 MPa*	Compressive strength of trial mix concrete test data after 13 weeks curing
Rebar	SD345 SD390 SD490	Strain 18% Strain 16% Strain 12%	Nominal value of JIS
Tendon		Strain 3%	Engineering judgement based on the tendon system test data of 3.8%
Liner		Strain 8%	Referring to 1/6 RCCV test

*30% reduction of these concrete failure criteria in the direction normal to initial concrete cracking direction

2.3 Wall-Basemat Juncture Analysis

2.3.1 Material Properties and Models

The shear stiffness under concrete cracking condition was reduced linearly to zero at 10 times of concrete crack strain, because shear failure was predicted in this region. All the other material properties were same with those in the global analysis.

2.3.2 Analytical Modeling

The axisymmetric model included part of the basemat with tendon gallery and containment walls. The basemat portion of the model was surrounded by the curved and upper surface of the basemat and tendon-gallary-symmetory lines of

each.

Concrete was modeled with axisymmetric solid element (CAX4). Rebar, tendon, and vertical liner anchor were defined as reinforcement (REBAR) in solid element. Concrete was, as shown in Fig. 6, simulated by duplicate elements of concrete and elastic body having 1/1000 stiffness of concrete, where REBAR element was defined in the elastic body. The concrete element was deleted to continue the analysis under high-pressure condition and to avoid calculation termination by divergence after reaching the stress of zero due to concrete cracking. Figure 7 shows concrete elements deleted after reaching quite small meridional stress at the shown pressure level. Sheath was not modeled because tendon was not allowed to slip. Liner and liner anchor were modeled with shell element (SAX1). The model consisted of t 2194 elements and 1159 nodes.

As boundary conditions, the vertical displacement and radial displacement of the global analysis were imposed on boundary surfaces. After the tendon prestressing, internal pressure was imposed.

2.3.3 Analysis Results

Figure 8 shows concrete cracking behaviors of the model. Vertical cracking (cracking due to vertical stress) first occurred at the left side corner of tendon gallery and inner corner of the junction at 1.5 Pd. The former occurred as a result of the shear force in the upper region of tendon gallery which was pulled upwards. The latter was governed by the shear force in the cylinder part deformed by internal pressure; cylinder part was deformed more easily than basemat. Hoop cracking initially occurred at 2.2 Pd near upper boundary surface, similar to global analysis as shown in Fig. 3. The cracking region was extended as pressure increased. At 3.2 Pd, vertical cracking extended to tendon gallery, and so did hoop cracking to the whole cylinder region.

Figure 9 plots vertical liner strains compared with global analysis results at two locations. The vertical liner strain at el. 250 mm, below horizontal liner anchor, was

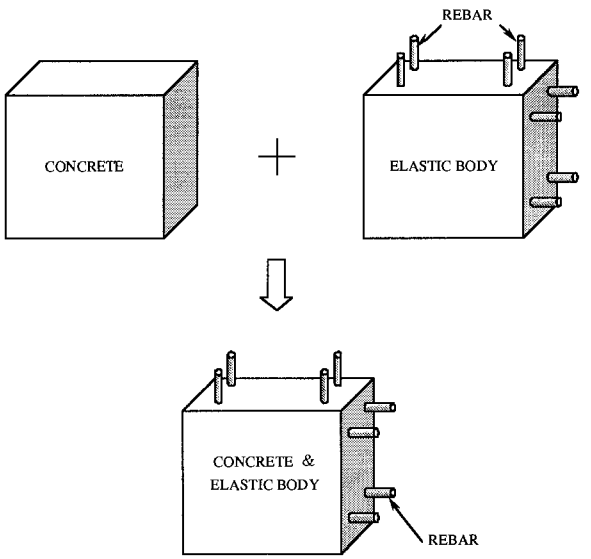

Fig. 6 Duplicate Concrete Modeling

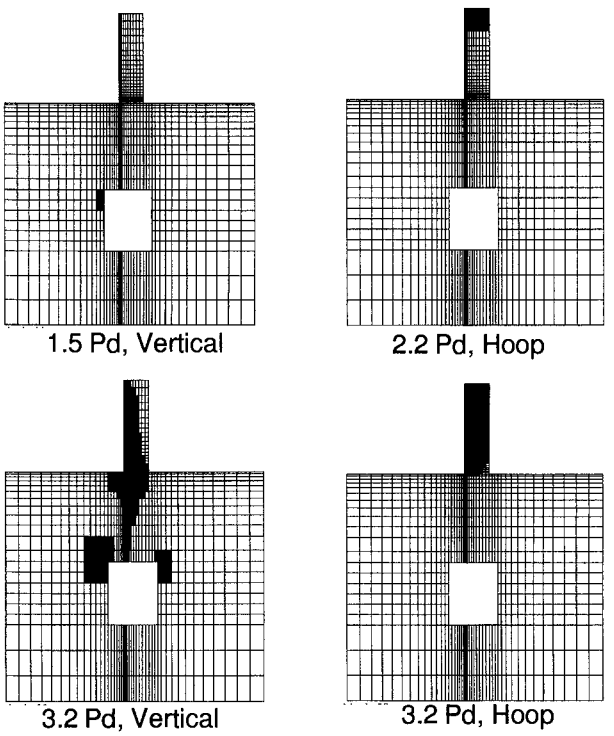

Fig. 8 Concrete Cracking

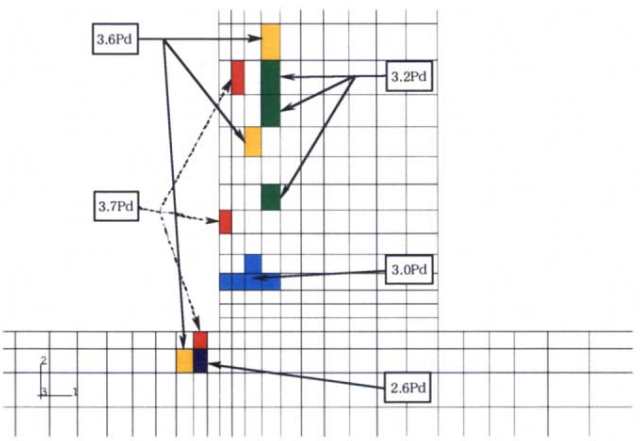

Fig. 7 Deleted Concrete Elements

smaller than the strain of the global analysis result. The liner anchor, which was not modeled in the global analysis, restrained the strain. The liner strain at el. 1000 mm, close to the model boundary, was similar to that of global analysis due to small influence of liner anchor. The strains at all locations of the analysis were less than 0.25%. Therefore, probability of liner tearing up to about 3.8 Pd was anticipated to be small.

Figure 10 shows principal compressive stress under the pressure of 3.74 Pd. The maximum compressive stress of 67 MPa at the outside of the junction was calculated. If the reduction of failure criteria normal to initial concrete cracking direction is assumed to be 30%, the failure criteria becomes 34 MPa. However, only 4 elements exceeded the 34 MP, not extending beyond rebar layer. Therefore, the probability of concrete shear failure at this location up to about 3.8 Pd was expected to be small.

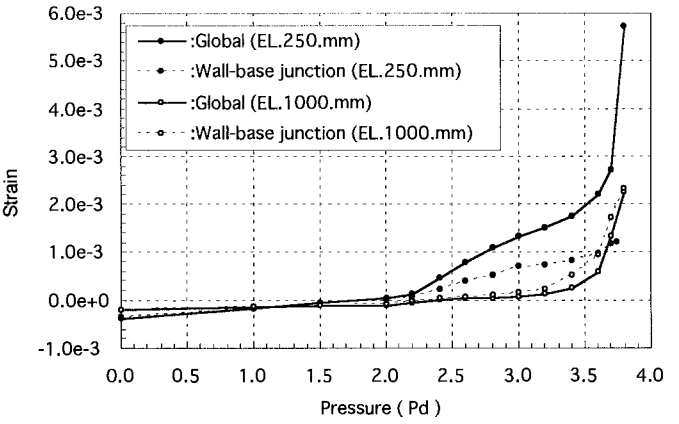

Fig. 9 Vertical Liner Strains

2.4 Equipment Hatch Analysis

2.4.1 Analytical Modeling

Figure 11 shows the model, which extended from the center of the equipment hatch (E/H) to 4500 mm above vertically and from buttress center to 90 degrees horizontally. The vertical displacement of the global analysis was applied to both upper and lower surfaces. Displacement in hoop direction of both of the side surfaces was fixed. Since two vertical adjacent tendons in the model should be considered as one set, the tensile forces of two adjacent tendons in the set had same value at the plane of symmetry on the opposite side of the buttress.

Concrete was modeled with solid element (C8D8). Rebar and vertical tendon were modeled with reinforcement (REBAR) in solid element. Concrete was simulated by duplicate elements of concrete and elastic body with rebars, same as those in the wall-base junction analysis. Sheath for vertical tendon was not modeled, the slip being not allowed. Hoop tendon and its sheath were modeled with 2-node beam element (B31). Contact element (ITT31) was placed between tendon and sheath so that hoop tendon could slip. Friction coefficient between tendon and sheath was not constant, modeled by the correlation depending on tendon end force and the angle from the tendon end [6], [7]. Liner, sleeve, and hatch cover were modeled with shell element (S4). Liner anchor was not modeled. The model consisted of 16,567 elements and 9,172 nodes.

As for meridional tendon, initial stress of the design value of setting condition was imposed. Hoop tendon was prestressed with the design value, and then loosed to the measured value in ancillary test performed.

All concrete elements were deleted at 2.8 Pd, after hoop stress of concrete reaching almost zero.

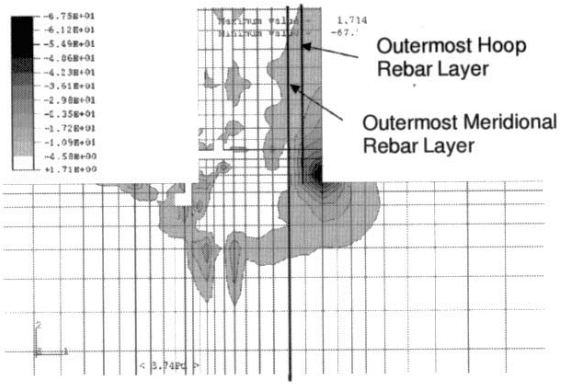

Fig. 10 Principal Compressive Stress (3.74 Pd)

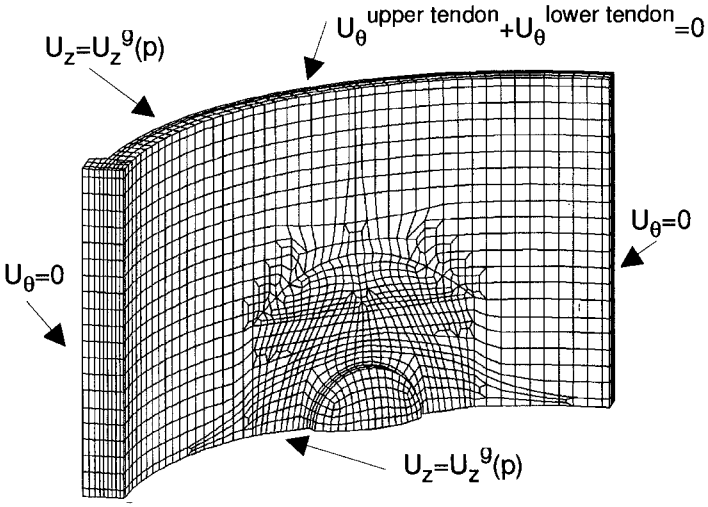

Fig. 11 Equipment Hatch Model

2.4.2 Analysis Results

Figure 12 plots radial displacements at two locations compared with a global analysis result. The displacement of free field was similar to that of global analysis, which showed the validity of modeling of this local analysis. The displacement of hatch cover center increased drastically after concrete hoop stress had reached basically zero and all the concrete elements had been deleted.

Figure 13 shows principal tensile strain of liner under several pressures. Principal strain concentrated in upper region of hatch cover at 1.0 Pd. The principal tensile strain concentrated also in buttress and discontinuous position of concrete thickness at 2.2 Pd because of concrete cracking. At 3.8 Pd, the principal strain of discontinuous position became larger than that of buttress. The maximum strain reached 3.5% at 4.0 Pd, which was much less than 8% of liner failure strain. That is, liner tearing was not predicted up to 4.0 Pd around E/H. On the other hand, tendon strain reached 3.2% in the vicinity of tendon end at 4.0 Pd, which was larger than 3% of tendon failure strain. That is, tendon rupture was predicted at 4.0 Pd near equipment hatch.

2.5 Main Steam Nozzles Analysis

Modeling methods and boundary conditions were same with those for the equipment hatch analysis.

Figure 14 shows principal tensile strain of the model. At 1.0 Pd, strain concentrated in sleeves in a similar fashion with the equipment hatch model. At 2.0 Pd, the maximum principal strain was around buttress, with strain concentration also around the place where rebar number changed. At 4.0 Pd, the maximum strain reached 6%, located at the place where rebar number changed. The strain, 6%, was smaller than the failure criteria of the liner, 8%; thus, the possibility of liner rupture was expected to be small.

3. CONCLUSION

According to the axisymmetric global analysis as the first step of the pretest analyses, concrete crack, occurring at about 2.0 Pd, remarkably increased rebar/tendon stress in the cylinder part. At 3.7 Pd, the stress of concrete became almost zero, and the stress of rebar became nearly uniform because of the yielding. The stress of tendon also became nearly uniform in the cylinder part because of its yielding. Hence, the displacement increased in the radial direction remarkably.

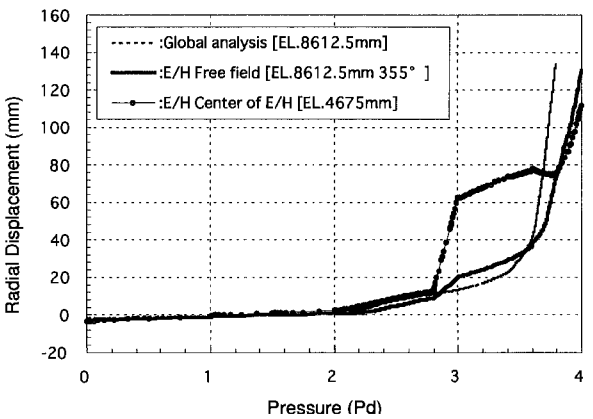

Fig. 12 Radial Displacements

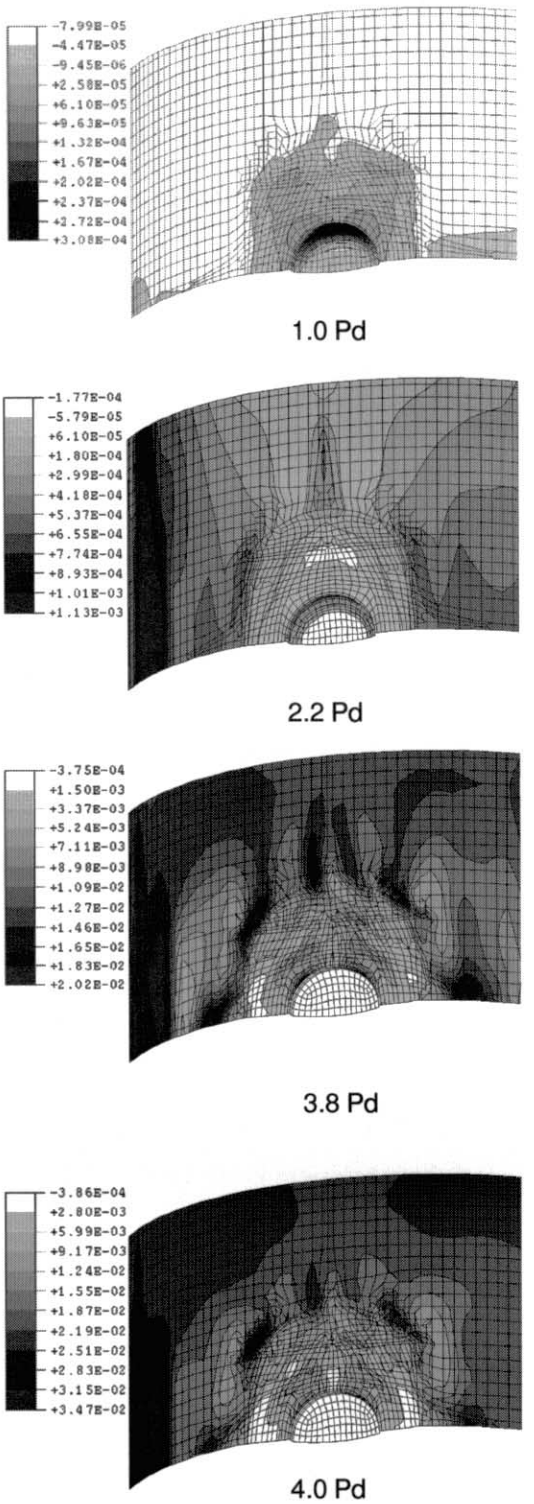

Fig. 13 Liner Principal Tensile Strain

In short, concrete cracking governed the global behavior of 1/4 PCCV model. That is, the reduction of concrete stress due to cracking caused the change in stress distributions of rebars and tendons and resultant global deformation behavior. The results well showed global behavior of the model and served as boundary conditions for the following local analyses.

Local analyses were conducted at 4 parts, wall-base junction, equipment hatch, air lock, and main stream nozzles where the failure had been predicted, three of which are discussed in the present paper.

According to the wall-base junction analysis with the axisymmetric model, the probability of liner tearing up to about 3.8 Pd and concrete shear failure at the juncture up to about 3.8 Pd was anticipated to be small.

In the equipment hatch analysis with a 3-D model, the principal tensile strain concentrated in buttress and concrete thickness discontinuity. Liner tearing was not predicted up to 4.0Pd around E/H. Tendon rupture was predicted at 4.0 Pd near equipment hatch, reaching 3.2% near tendon end at 4.0 Pd, which was larger than 3% of tendon failure strain.

In the main steam nozzle analysis with a 3-D model, the principal tensile strain concentrated around discontinuous position of rebar amount. The maximum principal strain was 6% at 4.0 Pd, not indicating high possibility of failure. However, it was the largest strain among the results, showing the highest possibility of liner failure.

In summary, the 1/4 PCCV model was predicted to fail by hoop tendon rupture in the mid-cylinder part between 3.8 Pd and 4.0 Pd. However, probability of liner tearing at the discontinuous position of concrete thickness still exists, if tendon rupture is not occurred.

A further direction of this study will be to compare analysis results with test results and to study analytical methods for the model and actual PCCV.

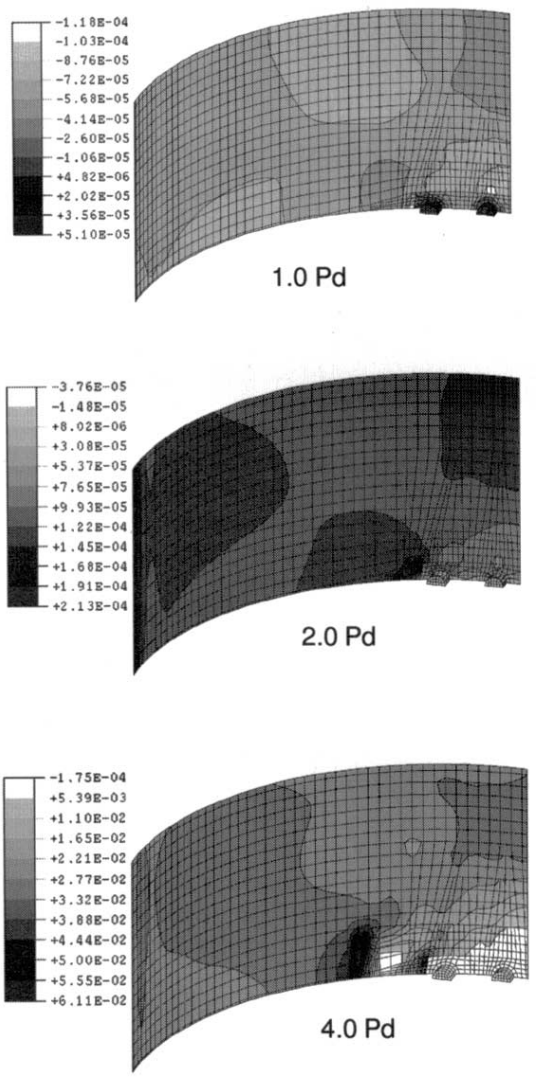

Fig. 14 Liner Principal Tensile Strain

ACKNOWLEDGMENT

This program is jointly sponsored by the Nuclear Power Engineering Corporation and the US Nuclear Regulatory Commission. The work of the Nuclear Power Engineering Corporation is performed under the auspices of the Ministry of Economy, Trade and Industry, Japan.

REFERENCES

1. Luk, V.K., *Pretest Round Robin Analysis of a Prestressed Concrete Containment Vessel Model (NUREG/CR-6678)*, U.S. Nuclear Regulatory Commission (NRC), DC, 2000
2. Hessheimer, M.F., Luk, V.K., Klamerus, E.W., Shibata, S., Mitsugi, S., and Costello, J.F., "Pretest Round Robin Analysis of 1:4-Scale Prestressed Concrete Containment Vessel Model," *Proc. Of the Ninth International Conference On Nuclear Engineering (ICONE 9)*, Nice, France, April 2001.
3. Horschel, D.S., 1992, *Experimental Results from Pressure Testing A 1:6-Scale Nuclear Power Plant Containment (NUREG/CR-5121)*, U.S. NRC, DC, 1992
4. Luk, V.K., Hessheimer, M.F., Hashimoto, T., and Costello, J.F., "Steel Containment Vessel Model Test: Results and Evaluation," Transaction of SMiRT-15, H06/5, pp 267-274, Seoul, Korea, August 1999.
5. Vecchio, F.J. and Collins, M.P., "The Modified Compression-Field Theory or Reinforced Concrete Elements Subjected to Shear," *ACI Journal*, March-April, 1986
6. Kashiwase, T. and Nagasaka, H., "Analysis Study on Change of Tendon Tension Force Distribution during the Pressurization Process of Pre-stressed Concrete Containment Vessel," *Proc. Of ICONE 5*, Nice, France, May 1997.
7. Kashiwase, T, and Nagasaka, H., 1998, "Extension of Tendon Friction Coefficient within Elastic Region to Plastic Region," *Summaries of Technical Papers of Annual Meeting - Architectural Institute of Japan*, Vol. B-2, pp 1113-1114, Kyushu, Japan, September 1998.